Journal of Molecular Catalysis A: Chemical 331 (2010) 7–14

Contents lists available at ScienceDirect

Journal of Molecular Catalysis A: Chemical

journal homepage: www.elsevier.com/locate/molcata

Editor's Choice paper

Surface hybridization effect of C_{60} molecules on TiO_2 and enhancement of the photocatalytic activity

Liwu Zhang, Yajun Wang, Tongguang Xu, Shengbao Zhu, Yongfa Zhu*

Department of Chemistry, Tsinghua University, Haidian District, Beijing 100084, PR China

ARTICLE INFO

Article history:
Received 1 June 2010
Received in revised form 27 July 2010
Accepted 29 July 2010
Available online 12 August 2010

Keywords:
Photocatalytic
C_{60}
Hybridization
Titanium dioxide

ABSTRACT

An efficient TiO_2 photocatalyst was obtained by surface hybridization with a thin layer of C_{60} molecules. The photocatalytic performance of C_{60}-hybridized TiO_2 under ultraviolet light irradiation was enhanced by 4 times compared with that of P25-TiO_2 photocatalyst. The enhanced photocatalytic activity for C_{60}-hybridized TiO_2 was originated from the high migration efficiency of photo-induced electrons on the interface of C_{60} and TiO_2, which was produced by the interaction TiO_2 and C_{60} with a conjugative π-system. The interaction was confirmed by the Raman spectroscopy, infrared spectroscopy and photoelectrochemical measurements. The enhancement of photocatalytic activity strongly depended on the coverage of C_{60} molecules on the surface of TiO_2, and the optimum hybridization effect was found at a weight ratio of 2.5 wt% (C_{60}/TiO_2). The mechanism for the enhanced photocatalytic activity of TiO_2 by C_{60} was discussed.

1. Introduction

Semiconductor photocatalysts have been attracted extensive attention for the destruction of environmentally hazardous chemicals and bioparticulates because of their cost-effective and complete mineralization without generation of toxic byproducts [1–3]. However, the potential for such applications is limited by low quantum efficiency. In the photocatalysis process, photogenerated electron–holes under irradiation migrate to the surfaces and take part in redox reactions generating reactive species such as hydroxyl radicals. At the same time, the recombination of electrons and holes is a major drawback which reduces the quantum efficiency of photocatalysis. Therefore, the photocatalytic activity of TiO_2 is not high enough for decomposition of high concentration pollutants due to low efficient. The commercialization of this technology in environmental remediation has been hindered [4–6]. Several attempts have been made to enhance the separation efficiency of photogenerated electrons and holes in order to reduce recombination, including C, N, S non-metal element doping [7–12], conjugating with electron scavenging agents [13–15], coupling of photocatalysts [16,17]. But the improvement of photocatalytic efficiency is far from satisfying. Therefore, the development of new materials for modifying TiO_2 is urgently needed to increase the photocatalytic activity of TiO_2 for organic pollutant treatment.

Conjugated material is proposed to be a good candidate for improving the transportation of photocarriers in the photocatalysis process by forming electronic interaction with TiO_2 due to its unique properties in electron or hole transporting [18–22]. Among them, fullerene has a variety of special chemical and physical properties due to the delocalized conjugated structure and has been studied quite extensively [19]. C_{60} can efficiently promote a rapid photo-induced charge separation and slow down charge recombination in dark. Therefore, C_{60} has been used to raise the performances of solar cell and medicinal chemistry [23,24]. Kamat et al. have demonstrated the charge transfer between C_{60} clusters and titanium dioxide under visible light, C_{60} can be reduced by one-electron in colloidal TiO_2 suspensions and form C_{60}^- [25–27]. Besides, many works focused on improving the efficiency of dye sensitization-based photochemical solar cells by adding C_{60} [27,28]. Those researches were mostly focused on the electron transfer between TiO_2 particle and C_{60} cluster. The photon-conversion efficiency can be improved by C_{60} cluster due to high separation efficiency for the photo-induced electrons and holes. Although use of fullerenes for scavenging photogenerated electrons from titanium dioxide particles has been demonstrated, a few efforts are made to utilize the unique properties of fullerenes to increase the efficiency of photocatalysis [21,29], however, the interior mechanism is yet not very clear, systematical study on a purpose of understanding the interaction between C_{60} molecular and TiO_2 and further effect on the photocatalytical activity is still necessary and important.

In this work, C_{60}-hybridized TiO_2 photocatalyst showed significantly enhanced photocatalytic activity for the degradation of

* Corresponding author. Tel.: +86 10 6278 3586; fax: +86 10 6278 7601.
E-mail address: zhuyf@mail.tsinghua.edu.cn (Y. Zhu).

1381-1169/$ – see front matter © 2010 Elsevier B.V. All rights reserved.
doi:10.1016/j.molcata.2010.07.015

salicylic acid and formaldehyde under UV-light irradiation. The enhancement of photoactivity was attributed to the enhanced interfacial charge separation between C_{60} layers and TiO_2 particles. The interaction between TiO_2 and C_{60} was investigated systematically. This surface modification method is very simple and could be used as a universal pathway to improve the activity of photocatalyst and applied in the environmental remediation.

2. Experimental

2.1. Preparation of C_{60}-hybridized photocatalyst

High-purity (99.99%) C_{60} sample was provided by Peking University, P.R. China. Particulate TiO_2 (particle diameter 30 nm, surface area 50 $m^2\,g^{-1}$) was obtained from Degussa Corp (P25). The preparation of C_{60}-hybridized TiO_2 samples was as follows: a known amount of C_{60} was added into toluene solution and ultrasonicated for 30 min to make C_{60} totally dissolve. 1 g of TiO_2 powder was added to the toluene solution containing C_{60} and was stirred for 24 h. And then the solvent was evaporated off. The opaque powder was then transferred to oven to dry at 80 °C for 12 h. In this present work, different mass ratio of C_{60}/TiO_2 from 1.25 to 7.5 wt% was made. The TiO_2 film was prepared on ITO glasses (1.5 cm × 2.0 cm) via a dip-coating method. The cleaned ITO glass was covered on two parallel edges with adhesive tape to control the thickness of the film and to provide a noncoated area for electrical contact. The TiO_2 film was dipped into a known amount of C_{60} toluene solution for 20 h, then taken out and dried at 80 °C for 12 h to obtain $ITO/TiO_2/C_{60}$ film samples.

2.2. Characterization

Ultraviolet-visible diffuse reflectance spectra (UV–vis DRS) were obtained by diffuse reflectance spectroscopy by using a Hitachi U-3010 instrument. Thermogravimetry (TG) and differential thermal analysis (DTA) analyses were performed on a thermal analyzer (DuPont 1090) under N_2 atmosphere with the heating rate of 5 °C min^{-1}. Raman spectra were recorded on a microscopic confocal Raman spectrometer (Renishaw 1000 NR) with an excitation of 514.5 nm laser light. Only 1 mW of the laser power was focused (spot size 5 mm) at the sample to avoid any optical damage or any nonlinear effects at the focused spot. The scattered light was collected in the 180° backscattering geometry. With this setup it is possible to monitor the Raman spectra with a spatial resolution of 5 mm. Spectra were collected in the range of 200–2000 cm^{-1} with a resolution of 1 cm^{-1}. HRTEM images were obtained by JEM 2010F field emission gun transmission electron microscope operated at an accelerating voltage of 200 kV. Samples for HRTEM measurements were prepared by ultrasonically dispersing the products into absolute ethanol, then placing a drop of this suspension onto a copper grid coated with an amorphous carbon film, and then drying in air. Electrochemical and photoelectrochemical measurements were performed in a home made three electrode quartz cells. Pt sheet was used as counter and Hg/Hg_2Cl_2/sat. KCl used as reference electrodes, while the working electrode was the thin film on ITO for investigation. The photoelectrochemical experiment results were recorded with a CHI 660B electrochemical system.

2.3. Photocatalytic measurements

The photocatalytic activities were tested for the degradation of salicylic acid in aqueous solution under UV light. 11 W germicidal lamp (λ = 254 nm) was used as the light source and the average light intensity was 1 mW cm^{-2}. Then 0.10 g of a photocatalyst was suspended in a 200 mL aqueous solution of 30 mg L^{-1} salicylic acid. Prior to irradiation, the suspensions were magnetically stirred in dark for about 30 min to reach the absorption–desorption equilibrium. At given time intervals, 3 mL aliquots were sampled and centrifugated to remove the particles. The filtrates were analyzed by recording variations of the maximum absorption band (295 nm for salicylic acid) on a Hitachi U-3010 UV-Vis spectrophotometer. In addition, the photocatalytic activities of the samples were also evaluated by the degradation of formaldehyde (FAD) in a closed quartz glass cell (250 mL) under ultraviolet irradiation. 0.05 g C_{60}-hybridized TiO_2 photocatalysts were evenly dispersed on a 7.5 cm × 2.5 cm quartz glass and then were put into the cell. A mixture which contains FAD of about 1800 ppm was then forced into the photoreactor. The concentration change of FAD in the sealed photoreactor was measured by a gas chromatograph with a flame ionization detector and a 2 m stainless steel column at 373 K. A UV-light lamp of 11 W (λ = 254 nm, Institute of Electric Light Source, Beijing) was used to provide UV-light source. The distance between the film and the light source was 5 cm, where the light intensity was measured to be 20 mW cm^{-2}. The concentration of formaldehyde was monitored on gas chromatograph (SP-502) with a flame ionization detector (FID). Both reactions were also carried out on TiO_2 (Degussa, P25) with a BET surface area of 55 m^2/g.

3. Results and discussion

3.1. Photocatalytic activities

The photocatalytic activities of C_{60}-hybridized TiO_2 were evaluated by the degradation of salicylic acid in aqueous solution and gaseous formaldehyde. Photodegradation of salicylic acid was carried out in air-equilibrated solutions. Fig. 1A shows the photodegradation of salicylic acid by C_{60}-hybridized TiO_2 under UV irradiation. For comparison, the photocatalytic activity of TiO_2 (P25) was also measured under identical conditions. Results showed that the adsorption of salicylic acid by TiO_2 was not appreciable within 2 h. No observable degradation of salicylic acid over TiO_2 (P25) or C_{60}-hybridized TiO_2 was observed in dark. It can be seen that only less than 5.0% of salicylic acid is degraded when illuminated under UV light (k_{app} = 0.0097 min^{-1}) without photocatalysts. However, all the C_{60}-hybridized TiO_2 samples exhibited higher photocatalytic activities for the degradation of salicylic acid under UV irradiation than that of pristine TiO_2. The photocatalytic activity was enhanced gradually with increasing the proportion of C_{60}. The photodegradation rate of photocatalytic reaction was influenced by the amounts of C_{60}-hybridized. Fig. 1B shows the comparison of the apparent rate constants k_{app} for the as-prepared photocatalysts with different ratio of C_{60}/P25. When the mass amount of C_{60} in the composites (TiO_2/C_{60}) was lower than 2.5 wt%, the value of k_{app} increased rapidly. However, with further increase of the C_{60} content in the composites, the photocatalytic activity decreases gradually. It is clear that the optimum content of C_{60} in the composites is 2.5 wt%. The photocatalytic activity of C_{60}-hybridized TiO_2 sample (2.5 wt%) increased by 4.0 times (k_{app} = 0.0410 min^{-1}) compared with that of P25. Hence, the coverage of C_{60} on the surface of TiO_2 could greatly enhance the photocatalytic activity of photocatalysts. As known, the photocatalytic activity was determined by various factors such as surface area, phase structure, and crystalline size and pore size [30,31]. In these cases, the above factors are all similar for TiO_2 and could not lead to the apparent difference for the photocatalytic activity. XRD patterns of TiO_2 showed no change before and after modification by C_{60}, indicating the absorption of C_{60} did not influence the lattice structure of TiO_2. No XRD diffraction peaks assigned to C_{60} were observed because the C_{60} layer was too thin. Moreover, there was no appreciable change in the surface area (BET surface area of TiO_2 and C_{60}-modified TiO_2 was 55 and 53 $m^2\,g^{-1}$,

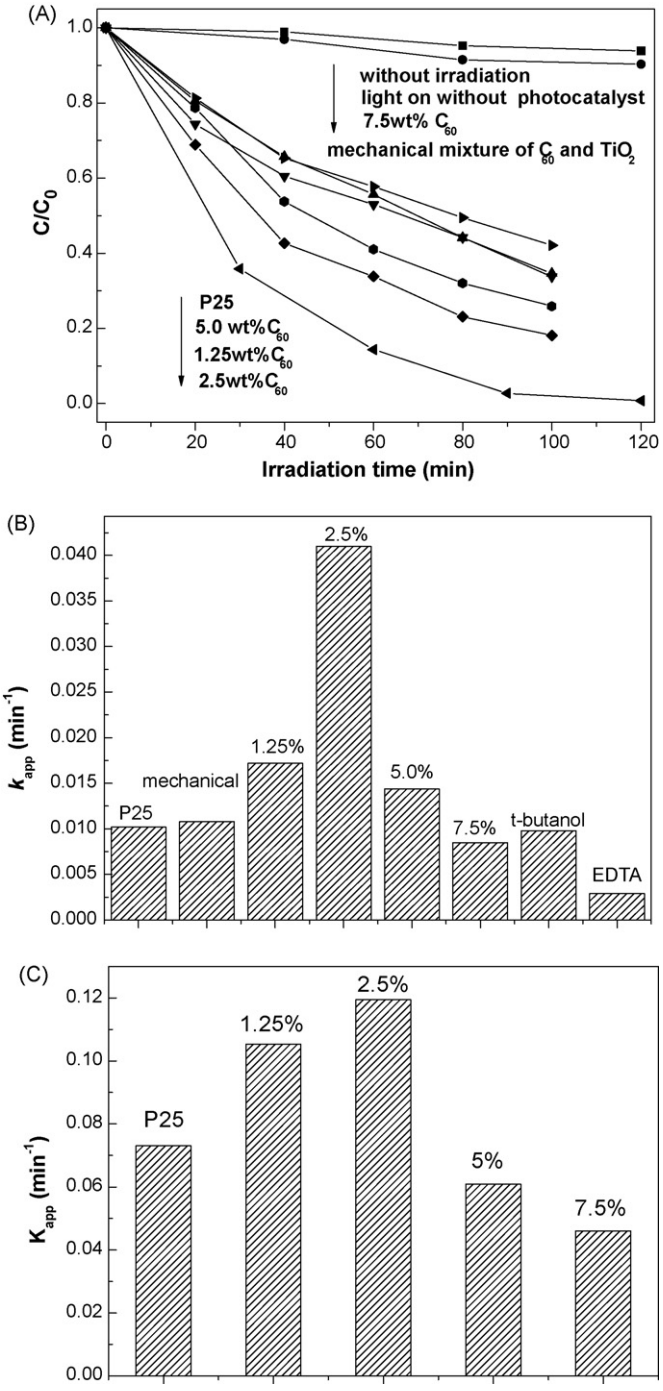

Fig. 1. (A) Photocatalytic degradation of salicylic acid by C_{60}-hybridized TiO_2 and TiO_2(P25) under UV-light irradiation. (B) First-order kinetic rate constants (k_{app}) for the photodegradation of salicylic acid with different photocatalysts under UV irradiation. (C) Photocatalytic degradation of formaldehyde by C_{60}-hybridized TiO_2 and P25 under UV-light irradiation.

respectively). Since the surface area and phase structure of TiO_2 remained almost the same before and after being modified by C_{60}, it can be inferred that the increasing of photocatalytic activities for composite photocatalysts should be resulted from the hybridization effect between the C_{60} layers and TiO_2 photocatalysts. This result implied that the interaction between C_{60} and TiO_2 photocatalyst played a crucial role in the enhanced photocatalytic activity of TiO_2 (P25), promoting the separation efficiency of electron and hole pairs. Furthermore, C_{60}-hybridized TiO_2 sample showed higher activity for degradation gas phase pollutants such as formaldehyde under UV-light irradiation (Fig. 1C). Similar to the result of salicylic acid degradation, the photocatalytic activity of C_{60}-hybridized TiO_2 samples exhibited higher photocatalytic activity. The C_{60}-hybridized TiO_2 samples also show higher activity than that of the mechanical mixture sample. However, the photocatalytic activity of the sample (7.5 wt%) was lower when the mass amount was beyond 5.0 wt%. The decreased activity with higher C_{60} content is considered to be related to increased absorbing and scattering of photons by surplus C_{60} in the photoreaction system. The coated C_{60} layers would shield the light reaching the surface of TiO_2 photocatalyst. Therefore, in order to get a high photodecomposition rate, a balance among these different effects of the C_{60} layers is crucial.

3.2. Structure and optical properties of C_{60}-hybridized TiO_2 photocatalysts

The high separation efficiency of charge carriers was mainly related to the interface structure of C_{60}/TiO_2 photocatalysts. The microstructure of C_{60}-hybridized TiO_2 was investigated by HRTEM. The typical lattice-resolved HRTEM image of C_{60}/TiO_2 (2.5 wt%) in Fig. 2 showed that the image of the inner had the obvious interplanar spacing of 0.35 nm, which corresponded to the (1 1 0) plane of TiO_2. And the lattice structure of TiO_2 sample after hybridized by C_{60} remains the same as that of TiO_2, no change can be found. However, it is very hard to confirm the existence of C_{60} from the HRTEM image.

The multi-molecular layer states of C_{60} on the surface of TiO_2 could be confirmed by the diffuse reflectance spectra. Fig. 3A shows the UV–vis diffuse reflectance spectra (UV–vis DRS) of C_{60}-hybridized TiO_2 samples. Only one absorption peak was shown in UV region below 400 nm for TiO_2. A wide absorption ranged from 200 to 700 nm was observed for all the C_{60}-hybridized TiO_2 samples compared with the absorption spectrum of TiO_2. The UV-DRS spectrum of C_{60}-hybridized TiO_2 was relatively broad and a new absorption peak emerged around 620 nm (inset of Fig. 3A). It was also found that the absorption edge was red-shifted for all the C_{60}-hybridized TiO_2 samples compared to the P25. It is also fount that the absorption intensity of the characteristic absorption band around 620 nm increased linearly with the amount of C_{60} increasing and the sample with 5.0 wt% C_{60} exhibited the largest absorption. Further increasing the amount of C_{60}, the intensity of absorption decreased slightly (Fig. 3B). This absorption at 620 nm is attributed to the C_{60} molecules on the surface of TiO_2. The decreased absorption intensity with C_{60} mass ratio higher than 5.0 wt% was interpreted as follows: the interaction between C_{60} and TiO_2 was chemical monolayer adsorption when the mass amount of C_{60} is less than 5.0 wt%, as the amount of C_{60} was more than 5.0 wt%, the monolayer coverage become saturation and some C_{60} molecules tended to form clusters on the surface of TiO_2 [25,26]. If we assumed the TiO_2 particles were ideal spheres, the mass ratio of C_{60} forming close-packed monolayer coverage on TiO_2(P25) was estimated about 11.8 wt% based on the fact that the diameter of C_{60} was 0.71 nm, and the surface area of P25 was about 50 $m^2\ g^{-1}$. In fact, C_{60} molecules could only occupy the active adsorption site on the surface TiO_2. Therefore, the actual mass ratio of C_{60} should be much less than 11.8 wt% for close-packed monolayer coverage. UV–vis diffuse reflectance spectra indicated that 5.0 wt% may be optimum for forming close-packed monolayer coverage.

Thermogravimetry and differential thermal analyses (TG–DTA) of C_{60}-hybridized TiO_2 samples (2.5 wt%) were shown in Fig. 4. For pristine P25-TiO_2, The weight loss (1.2 wt%) below 225 °C, which can also be found in C_{60}-hybridized TiO_2 sample, was attributed to the loss of water on the surface. The wide endothermic peak at about 225 °C may be attributed to the dehydroxylation of the –OH on the surface of TiO_2, the other endothermic peak at 530 °C was corresponded to the phase transformation of TiO_2. However, there

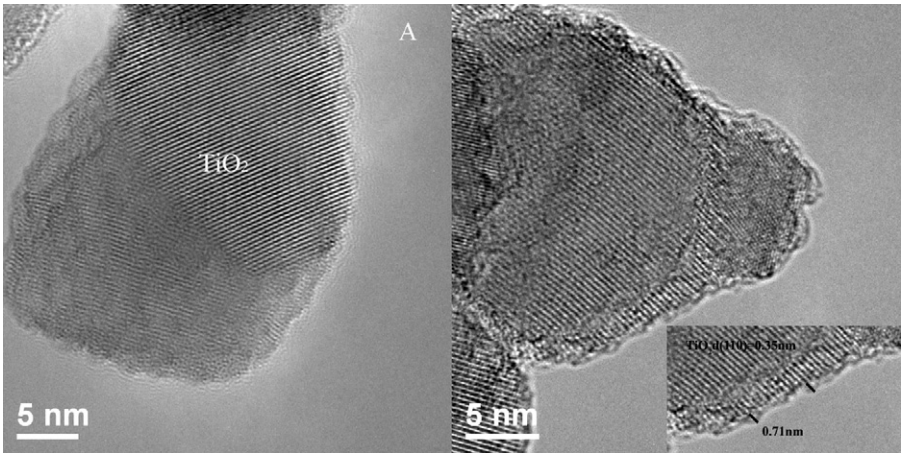

Fig. 2. HRTEM images of TiO_2 and C_{60}-hybridized TiO_2 samples (2.5 wt%).

were two different regions of weight loss for C_{60}-hybridized TiO_2 sample during the increase of temperature. The weight loss from 400 to 800 °C may be resulted from the chemical desorption of C_{60} molecules from the surface of TiO_2. The weight loss of this region was about 2.1 wt%, which was nearly consistent with the mass amount of C_{60} on the surface of TiO_2 (2.5 wt%). In DTA curve of C_{60}-hybridized TiO_2, the endothermic peak at 737 °C may be attributed to the chemical desorption of C_{60}. The exothermic peak at 660 °C should be related to the phase transition of TiO_2 from anatase to rutile [20], indicating that the phase transformation temperature of TiO_2 could be increased by surface hybridization with C_{60}, this effect is also found in some carbon modified TiO_2 reports [22].

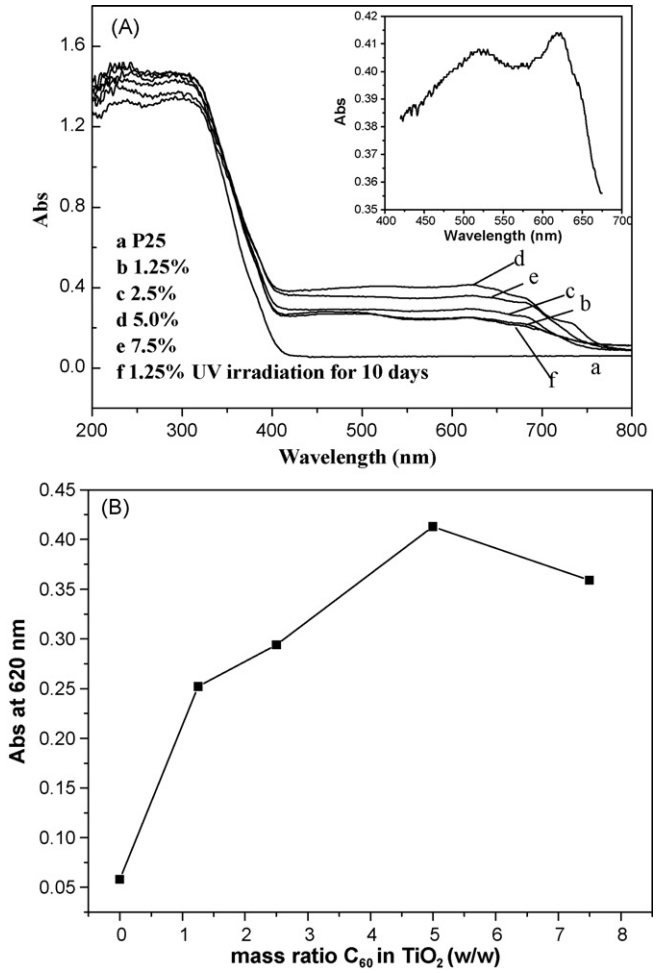

Fig. 3. (A) UV–vis diffuse reflectance spectra of TiO_2(P25) and C_{60}-hybridized TiO_2 with different mass ratio of C_{60}. Inset: diffuse reflectance spectrum of C_{60}-hybridized TiO_2 (2.5 wt%) in the wavelength region from 420 to 675 nm. (B) Changes of absorption (λ = 620 nm) from the DRS spectra as a function of mass ratio of C_{60}.

3.3. Photoelectrochemical performances

To investigate the electronic interaction between C_{60} and TiO_2, the photocurrent generated from the ITO/TiO_2/C_{60} electrode immersed in aqueous Na_2SO_4 solution was monitored. The time profiles of photocurrents generated under UV irradiation were shown in Fig. 5A. As illustrated, the TiO_2 and C_{60}-hybridized TiO_2 thin films were excited by absorbing UV light and subsequently transferred electrons into electrode to generate light-induced current. It can be found that the photocurrent of C_{60} (2.5 wt%)-hybridized ITO/TiO_2 film was about 4 times as high as that of ITO/TiO_2 film. This obvious enhancement of photocurrent for ITO/TiO_2/C_{60} film indicated that the separation efficiency of photo-induced electrons and holes was intensified by the electronic interaction between C_{60} molecular and TiO_2.

Fig. 5B shows the incident photon to current efficiency (IPCE) plot for C_{60}-hybridized TiO_2 film electrode in 0.1 M Na_2SO_4 com-

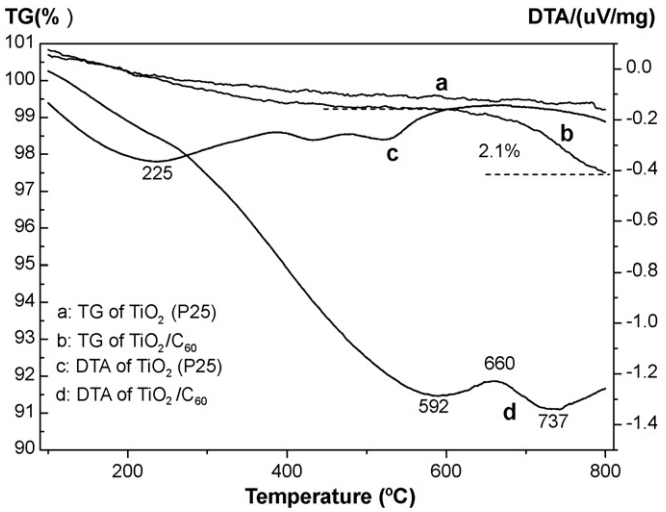

Fig. 4. TG and DTA curves of C_{60}-hybridized TiO_2 in the presence of N_2.

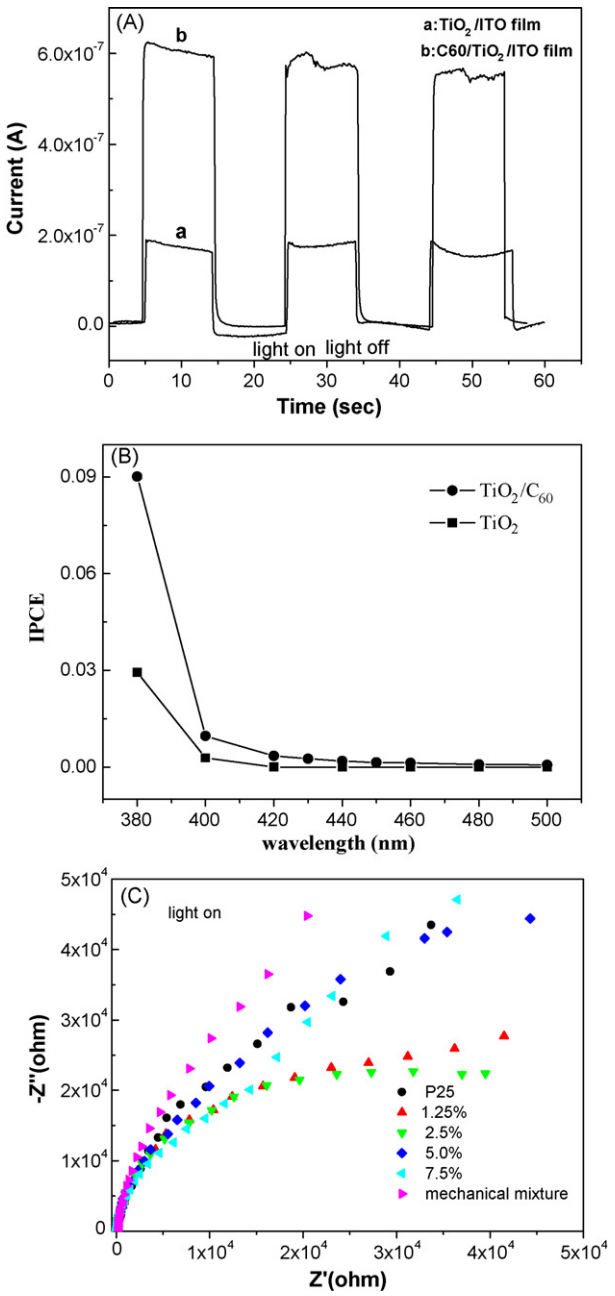

Fig. 5. (A) Photoelectrochemical response of ITO/TiO_2 and ITO/TiO_2/C_{60} thin films under UV-light irradiation (λ = 360 nm). The potential of the working electrode was set at 0.0 V *vs* the Pt counter electrode. (B) IPCE of TiO_2 and C_{60}-hybridized TiO_2 samples. (C) EIS response of the ITO/TiO_2/C_{60} thin films electrode under UV irradiation conditions.

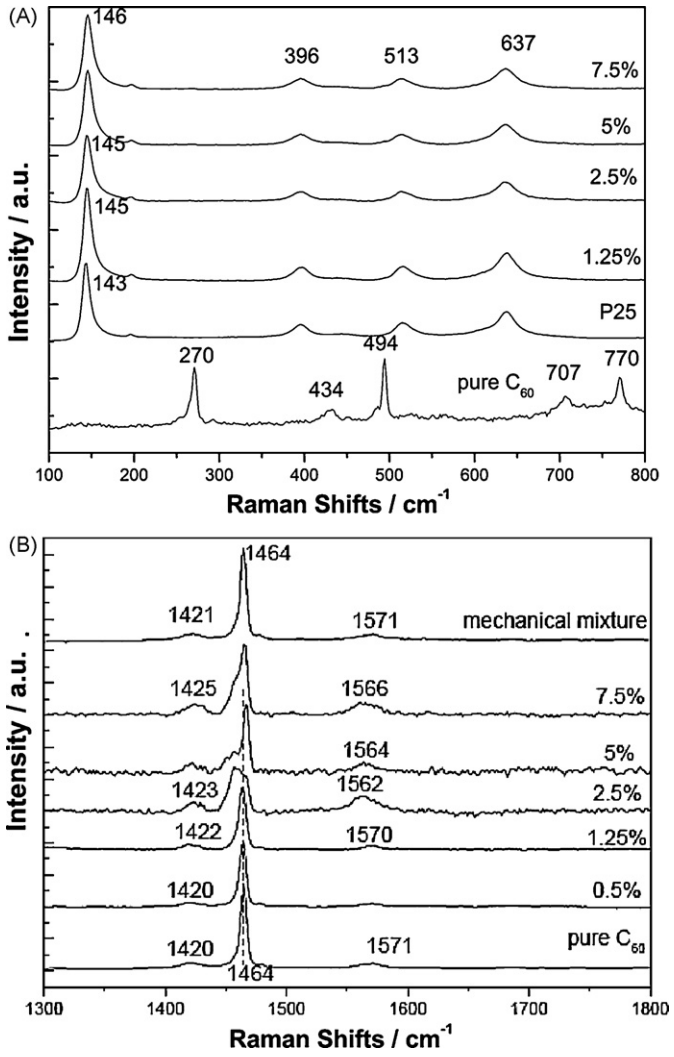

Fig. 6. Raman spectra of C_{60}-hybridized TiO_2, C_{60} and TiO_2 samples.

pared with that of a non-hybridized TiO_2 film. The onset of photocurrent was found at the wavelength of 400 nm for TiO_2 films. The photocurrent increased at excitation wavelength below this onset wavelength closely matched the absorption characteristics of TiO_2 (E_g = 3.2 eV), which indicated that the photocurrent was generated from TiO_2 in the thin film. A maximum IPCE about 9% was obtained at 380 nm. The IPCE under UV illumination was increased by 3 times with the hybridization of C_{60}. The higher IPCE of the ITO/TiO_2/C_{60}-hybridized electrode was therefore suggestive of increased charge separation in the composite film. The generation of anodic current indicated that the electrons flow to the surface of ITO [32]. These results also indicated that surface hybridization effect of TiO_2 photocatalyst by C_{60} enhanced the photo-induced charge separation efficiency greatly under UV irradiation.

A typical EIS response of illuminated C_{60}-hybridized TiO_2 electrodes obtained in the presence of Na_2SO_4 (0.1 M) was present in Fig. 5C. In each case, there was only one arc/semicircle on the EIS plane display, suggesting that the surface charge transfer was the rate-determining step in the photocatalytic reaction. A necessary step for semiconductor photocatalytic degradation was the generation and separation of electron–hole pairs. The smallest arc radius on the EIS Nyquist plot meaned an effective separation of the photogenerated electron–hole pair and a fast interfacial charge transfer to the electron donor/electron acceptor [33,34]. On the other hand, the C_{60} on the TNA surface reduced the UV absorption and the contacting area between the TiO_2 and solution, which decreased the utilization efficiency of light. The enhanced charge separation process and reduced efficiency of light are two compete factors in our system, which caused the photoelectric properties increased initially then decreased to the balance, and the highest photoresponse was obtained at 2.5 wt% C_{60} loaded, which also showed the highest activity in the photocatalytic degradation of salicylic acid.

Raman spectroscopy was applied to discriminate the local order characteristics of TiO_2 photocatalyst for its capability of elucidating the structural complexity as peaks separated in frequency from each material. Fig. 6A shows the Raman spectra of C_{60}, TiO_2 and C_{60}-hybridized TiO_2 samples. Most of the strong bands in the range of

100–800 cm^{-1} were mainly attributed to TiO_2. The Raman modes belonged to the anatase phase were presented in the spectra: B_{1g} (395 cm^{-1}), A_{1g} (519 cm^{-1}) and E_g (143, 195, and 637 cm^{-1}). The observed peaks in the range of 100–800 cm^{-1} for P25 were similar to those of bulk anatase with little upshift of frequency. It has been reported that the low-frequency peak (144 cm^{-1}) in anatase TiO_2 nanoparticles showed a strong dependence on the quantum size confinement effects [20]. In these cases, all the samples were not treated under high temperature, the TiO_2 possess the same particle size, therefore, the influence of quantum size effect can be excluded. These shifts of Raman peaks may be related to the close interaction between C_{60} and TiO_2.

The existence of fullerene in the composite materials was also identified by Raman spectroscopy. It is well-known that the Raman vibrational modes of the isolated C_{60} (I_h point group) molecule have 10 active bands: $H_g(1)$ (270 cm^{-1}); $H_g(2)$ (432 cm^{-1}); $A_g(1)$ (494 cm^{-1}); $H_g(3)$ (707 cm^{-1}); $H_g(4)$ (770 cm^{-1}); $H_g(7)$ (1420 cm^{-1}); $A_g(2)$ (1464 cm^{-1}) [35]. As shown in Fig. 6B, all the significant Raman lines of free fullerenes can be traced in this system, the Raman spectrum of pure C_{60} exhibited the strongest bands at 1464 and 494 cm^{-1} (A_g symmetry) and a number of weaker bands at 707, 770, 1248, 1420, 1490, and 1571 cm^{-1} (H_g symmetry). It was obvious that some changes occurred in the Raman spectrum after TiO_2 was hybridized with C_{60}, the $A_g(2)$ symmetry band at 1464 cm^{-1} was downshifted with the doping amount of C_{60} increasing. The largest downshift of this band is approximately 6 cm^{-1} in the case of 2.5 wt% C_{60}-hybridized TiO_2, whereas the 494 cm^{-1} band of $A_g(1)$ almost disappeared. This most characteristic Raman band at 1464 cm^{-1} for the $A_g(2)$ pentagonal pinch mode was related to the carrier transfer, as there was charge transfer to C_{60} molecules, the mode would shift to lower frequency [36]. These result further confirmed the electronic interaction between C_{60} and TiO_2.

At low coverage, the $A_g(2)$ mode appeared as a single peak at about 1464 cm^{-1}, similar with that of pure C_{60}. As the coverage increased, this mode was downshifted to the low frequency and the line widths increased. At the optimal coverage, a wider Raman shifts appeared at 1458 cm^{-1} modes in the sample (2.5 wt%). This coverage effect can only be the result of the strongest interaction of the C_{60} molecules with the TiO_2 surface which leaded to the most partial charge transfer [37]. As the coverage of C_{60} further increasing (5.0, 7.5 wt%), the $A_g(2)$ mode upshifted from 1458 to 1464 cm^{-1}, indicating the hybridization interaction between TiO_2 and C_{60} is weakened. The phenomena can be explained as follows: at the coverage of 2.5 wt%, the C_{60} molecules dispersed on the surface of TiO_2 with near-monolayer molecular states, stronger hybridization interaction with conjugated π system existed between the TiO_2 and C_{60} molecules. When the coverage was higher than 2.5 wt%, the aggregation of C_{60} molecules occurred on the surface of TiO_2 and formed C_{60} clusters, resulting in the decrease of hybridization interaction between TiO_2 and C_{60}. In addition, the Raman mode of mechanical mixture sample was similar with that of pure C_{60}, indicating that the interaction between TiO_2 and C_{60} molecules was mainly physical absorption for the mechanical mixture sample. Compared with the mechanical mixture of P25 and C_{60}, the $A_g(2)$ mode in some hybridized samples was shifted to lower frequency, indicative of stronger bonding and chemical interaction at the interface of C_{60} and TiO_2.

Selected parts of the IR spectrum of TiO_2, C_{60}, the C_{60}-hybridized TiO_2 photocatalyst (2.5 wt%) and the mechanical mixture of C_{60} and TiO_2 were shown in Fig. 7. The peaks at 527, 577, 1183, and 1428 cm^{-1} are fundamental IR active modes consistent with those previously reported literature and are attributed to the internal modes of the C_{60} molecule [38]. As comparison, there were no infrared peaks of TiO_2 overlapped with C_{60} in the range of

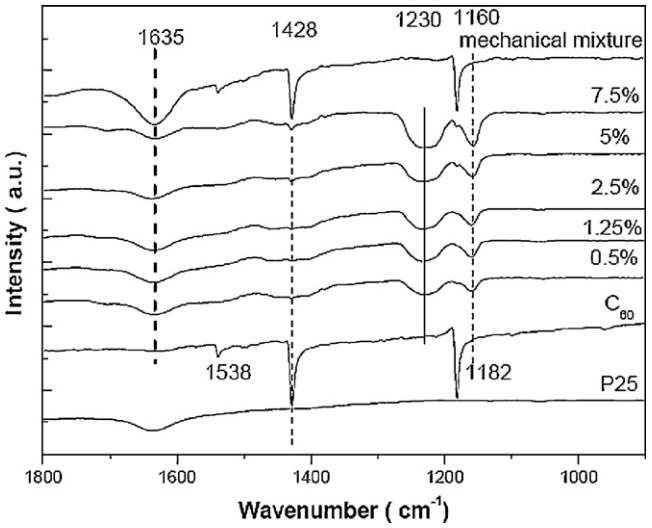

Fig. 7. FTIR transmission spectrum of TiO_2 samples hybridized by different amounts of C_{60} (0.5, 1.25, 2.5, 5.0, 7.5 wt%) and mechanical mixture of C_{60} and TiO_2.

1800–900 cm^{-1}, only one peak at 1633 cm^{-1} can be found in IR spectrum. The hybridization between TiO_2 and C_{60} molecules slightly changed the IR spectrum of C_{60}. The most prominent change was that the characteristic mode at 1182 cm^{-1} was split into two peaks at about 1225 and 1159 cm^{-1}. Moreover, the 1428 cm^{-1} peak gradually diminished and formed a wide peak including some weak peaks at 1448, 1427, 1403 and 1386 cm^{-1}. These two characteristic modes (1182 and 1428 cm^{-1}) are known for being sensitive to charge transfer of C_{60}, therefore, it can be concluded that the electronic interaction between TiO_2 and C_{60} induced the splitting and extension [39]. This assumption was further proved by the IR spectrum of the mechanical mixture of C_{60} and TiO_2, the spectrum of mechanical mixture remained the same as that of pure C_{60} molecules, no evident changes could be found indicating that the C_{60} molecules were absorbed on the surface of TiO_2 with physical interaction, while the chemical interaction existed in the TiO_2 samples hybridized with C_{60}.

3.4. Mechanism of the enhanced photocatalytic activity

The photodegradation of organic pollutants mechanism of TiO_2 photocatalyst under UV illumination has been investigated systematically. After photogenerated electron (e^-)–hole (h^+) pair in TiO_2 migrated to the surface of catalyst particles, there were two possible way for the photocatalytic reaction: the hole can directly reacted with surface adsorbed organic substrates; electrons were captured by chemisorbed OH^- or H_2O to produce •OH radical species which can react with organic substance [1,2]. The effect of alcohols on the photocatalytic rate of transformation has been interpreted in terms of discriminating between direct holes oxidation and reaction with radicals. Here *tert*-butanol was introduced to scavenge the radicals and investigated the role of free radicals and holes during the photodegradation process in the present of C_{60}-hybridized TiO_2 samples [40]. Results were shown in Fig. 8, it can be clearly seen that the presence of *tert*-butanol decreased the degradation rate of salicylic acid obviously which meant that *tert*-butanol scavenged the radicals during the reaction process. At the same time, the degradation of salicylic acid was still detectable, indicating that both free radicals and holes participated in the photocatalytic reaction for C_{60}-hybridized TiO_2 samples. On the other hand, the effect of EDTA, the trapper of the photogenerated hole [40], on the photocatalytic activity reaction rate was also studied. The photocatalytic degradation rate for the salicylic acid was

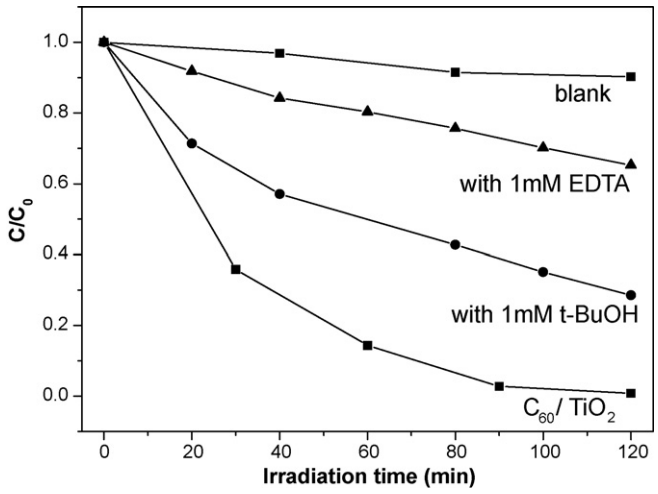

Fig. 8. The photocatalytic performance of hybridized P25 for the decomposition of (a) salicylic acid, (b) salicylic acid and *t*-butanol, (c) salicylic acid and EDTA.

greatly decreased in the presence of EDTA. This indicated that the photogenerated holes were the main active species in this system. From these above results, it can be concluded that radical oxidation and holes oxidation process coexisted in the photocatalytic reaction. The photocatalytic reaction of organic compounds in the C_{60}-hybridized TiO_2 system proceeded via both surface intermediates of oxygen reduction and direct reaction with holes.

The enhancement of photocatalytic activities was mainly due to the high efficiency of charge separation induced by the synergetic effect of C_{60} and TiO_2. The processes of photogenerated charge transition during photo-irradiation were shown in Fig. 9. In C_{60}-hybridized TiO_2 sample, hole and electron pairs were generated and separated on the interface of TiO_2 when illuminated by UV light. The level of conduction band in TiO_2 (−0.5 eV *vs* NHE) was lower than the reduction potential of C_{60} (−0.2 eV *vs* NHE) [25,26], Therefore, the photogenerated electron can easily emigrate from the conduction band of TiO_2 to C_{60} molecule with the interaction between TiO_2 and C_{60}. Monolayer C_{60} molecules played an important role in storing and shuttling photo-induced electrons generated from TiO_2 photocatalyst, which promoted the separation efficiency of photo-induced electron–hole pairs and decreased the recombination rate of electron–hole pairs. Because C_{60} were trap-rich conductors, the C_{60} molecules acted as an electron relay [41,42], the role of the injected electrons in this system was not simply to increase the density of charge carrier but also to fill trap states and hence increased the average mobility [24]. Moudjil and coworkers reported that C_{60} molecules absorbed on the surface of TiO_2 presented an immediate and direct route of electron transfer to C_{60} was directly from the TiO_2, and increased the rate of hydroxyl radical generation [21]. At the same time, the holes in valence band (VB) of TiO_2 can directly

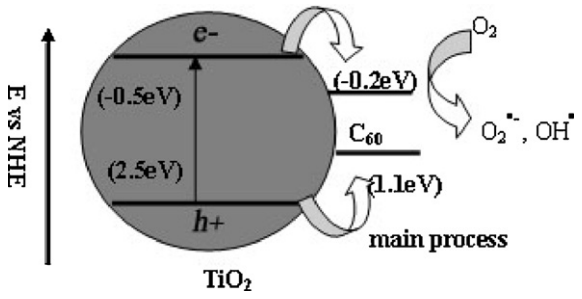

Fig. 9. Schematic drawing of separation of photogenerated electrons and holes on the interface of C_{60} and TiO_2.

transfer to the HOMO of C_{60}, because the VB of TiO_2 matched well with the HOMO of C_{60}. The synergetic effect C_{60} and TiO_2 both promoted the separation efficiency of photogenerated electron–hole pairs resulting in the high photocatalytic activity of C_{60}-hybridized TiO_2 samples. Hence, the modification method was an effective way to improve the photocatalytic activity and can also be applicable in other photocatalysts.

The photocatalytic activity was not only determined by the amount of C_{60} which transferred the photo-induced electrons, but also related to the contact area between TiO_2 and organic pollutants. The presence of optimum hybridized weight ratio of C_{60} to TiO_2 can be explained on the basis of surface coverage of TiO_2 nanoparticles by C_{60}. At a low coverage (0.5 wt%), few photogenerated electrons are scavenged by C_{60}. Further increasing the concentration of C_{60} leads to greater surface coverage and the number of scavenged photogenerated electron also increases, resulting in the higher photocatalytic activity (seen the sample with 1.25 wt% C_{60}). When the mass amount of C_{60} reached 2.5 wt%, the C_{60} molecules tended to completely dispersed on the surface of TiO_2 with near-monolayer coverage, resulting the most photogenerated electron–hole pairs [30,31]. The stability of C_{60}-hybridized TiO_2 photocatalyst under UV light was investigated (Fig. 3A curve f). After irradiated under UV light for 10 days, DRS spectra of C_{60}-hybridized TiO_2 changed very little, implying C_{60}-hybridized TiO_2 samples held good photostability under UV-light irradiation.

4. Conclusion

Multi-molecular layer C_{60}-hybridized TiO_2 photocatalysts have been prepared via a simple method. The as-prepared samples exhibited remarkably enhanced photocatalytic activity for the degradation of pollutants under UV irradiation. It appears that the electronic contact between semiconductor and C_{60} results in the efficient separation of electron–hole pairs to minimize the energy-wasteful electron–hole recombination, which leads to high photocatalytic activity under UV irradiation.

Acknowledgements

This work was partly supported by Chinese National Science Foundation (20925725, 20673065), National Basic Research Program of China (2007CB613303) and Chinese Postdoctoral Foundation (023215006).

References

[1] M.R. Hoffmann, S.T. Martin, W. Choi, D.W. Bahnemann, Chem. Rev. 95 (1995) 69–96.
[2] A.L. Linsebigler, G. Lu, J.T. Yates, Chem. Rev. 95 (1995) 735–758.
[3] M.A. Fox, M.T. Dulay, Chem. Rev. 93 (1993) 341–357.
[4] H. Kominami, S. Murakami, J. Kato, Y. Kera, B. Ohtani, J. Phys. Chem. B 106 (2002) 10501–10507.
[5] J.C. Yu, L. Zhang, Z. Zheng, J. Zhao, Chem. Mater. 15 (2003) 2280–2286.
[6] M. Addamo, V. Augugliaro, A. Di Paola, E. Garcia-Lopez, V. Loddo, G. Marci, R. Molinari, L. Palmisano, M. Schiavello, J. Phys. Chem. B 108 (2004) 3303–3310.
[7] R. Asahi, T. Morikawa, T. Ohwaki, K. Aoki, Y. Taga, Science 293 (2001) 269–271.
[8] H. Irie, Y. Watanabe, K. Hashimoto, J. Phys. Chem. B 107 (2003) 5483–5486.
[9] M. Mrowetz, W. Balcerski, A.J. Colussi, M.R. Hoffmann, J. Phys. Chem. B 108 (2004) 17269–17273.
[10] T. Ohno, T. Mitsui, M. Matsumura, Chem. Lett. 32 (2003) 364–365.
[11] J.C. Yu, G.J. Yu, W.K. Ho, Z.T. Jiang, L.Z. Zhang, Chem. Mater. 14 (2002) 3808–3816.
[12] J.C. Yu, W. Ho, J. Yu, H. Yip, P.K. Wong, J. Zhao, Environ. Sci. Technol. 39 (2005) 1175–1179.
[13] E.P. Reddy, B. Sun, P.G. Smirniotis, J. Phys. Chem. B 108 (2004) 17198–17205.
[14] E. Bae, W. Choi, Environ. Sci. Technol. 37 (2003) 147–152.
[15] C. Chen, P. Lei, H. Ji, W. Ma, J. Zhao, H. Hidaka, N. Serpone, Environ. Sci. Technol. 38 (2004) 329–337.
[16] X. Fu, L.A. Clark, Q. Yang, M.A. Anderson, Environ. Sci. Technol. 30 (1996) 647–653.
[17] W. Ho, J.C. Yu, J. Lin, G.J. Yu, P. Li, Langmuir 20 (2004) 5865–5869.

[18] W. Ma, C. Yang, X. Gong, K. Lee, A.J. Heeger, Adv. Funct. Mater. 15 (2005) 1617–1622.
[19] M. Reyes-Reyes, K. Kim, D.L. Carrol, Appl. Phys. Lett. (2005) 093506.
[20] S. Shanmugam, A. Gabashvili, D.S. Jacob, J.C. Yu, A. Gedanken, Chem. Mater. 18 (2006) 2275–2282.
[21] V. Krishina, N. Noguchi, B. Koopman, B. Moudgil, J. Colloid Interface Sci. 304 (2006) 166–171.
[22] L.W. Zhang, H.B. Fu, Y.F. Zhu, Adv. Funct. Mater. 18 (2008) 2180–2189.
[23] C.J. Brabec, A. Cravino, D. Meissner, N.S. Sariciftci, T. Fromherz, M.T. Rispens, L. Sanchez, J.C. Hummelen, Adv. Funct. Mater. 11 (2001) 374–380.
[24] R.T. Da, M. Prato, Chem. Commun. (1999) 663–669.
[25] P.V. Kamat, I. Bedja, S. Hotchandani, J. Phys. Chem. 98 (1994) 9137–9142.
[26] P.V. Kamat, M. Gevaert, K. Vinodgopal, J. Phys. Chem. B 101 (1997) 4422–4427.
[27] P.V. Kamat, M. Haria, S. Hotchandani, J. Phys. Chem. B 108 (2004) 5166–5170.
[28] E. Bustos, J. Manriquez, L. Echegoyen, L.A. Godinez, Chem. Commun. (2005) 1613–1615.
[29] Y. Long, Y. Huang, Y. Peng, Y. Lu, S. Kang, J. Mu, J. Phys. Chem. C 113 (2009) 13899.
[30] J.C. Yu, J.G. Yu, W.K. Ho, L.Z. Zhang, Chem. Commun. (2001) 1942–1943.
[31] J.C. Yu, J.G. Yu, L.Z. Zhang, W.K. Ho, J. Photochem. Photobiol. A 148 (2002) 263–271.
[32] K. Vinodgopal, I. Bedja, P.V. Kamat, Chem. Mater. 8 (1996) 2180–2187.
[33] W.H. Leng, Z. Zhang, J.Q. Zhang, C.N. Cao, J. Phys. Chem. B 109 (2005) 15008–15023.
[34] H. Liu, X.Z. Li, Y.J. Leng, W.Z. Li, J. Phys. Chem. B 107 (2003) 8988–8996.
[35] V. Schettino, M. Pagliai, L. Ciabini, G. Cardini, J. Phys. Chem. A 105 (2001) 11192–11196.
[36] L. Kavan, L. Dunsch, H. Kataura, A. Oshiyama, M. Otani, S. Okada, J. Phys. Chem. B 107 (2003) 7666–7675.
[37] X.L. Wu, F. Yan, X.M. Bao, S. Tong, G.G. Siu, S.S. Jiang, D. Feng, Phys. Lett. A 225 (1997) 170–174.
[38] S.G. Stepanian, V.A. Karachevtsev, A.M. Plokhotnichenko, L. Adamowicz, A.M. Rao, J. Phys. Chem. B 110 (2006) 15769–15775.
[39] M. Krause, D. Deutsch, P. Janda, L. Kavan, L. Dunsch, Phys. Chem. Chem. Phys. 7 (2005) 3179–3184.
[40] H. Lee, W. Choi, Environ. Sci. Technol. 36 (2002) 3872–3878.
[41] D.M. Guldi, M. Prato, Acc. Chem. Res. 33 (2000) 695–703.
[42] V. Krishna, D. Yanes, W. Imaram, A. Angerhofer, B. Koopman, B. Moudgil, Appl. Catal. B 79 (2008) 376–381.